Mon. Not. R. Astron. Soc. **000**, 000–000 (0000) Printed 17 June 2014 (MN LATEX style file v2.2)

Kinematical fingerprints of star cluster early dynamical evolution

Enrico Vesperini[1], Anna Lisa Varri[1,2], Stephen L.W. McMillan[3], Stephen E. Zepf[4]
[1] *Department of Astronomy, Indiana University, Bloomington, IN 47405, USA*
[2] *School of Mathematics and Maxwell Institute for Mathematical Sciences, University of Edinburgh, Edinburgh EH9 3JZ, UK*
[3] *Department of Physics, Drexel University, Philadelphia, PA 19104, USA*
[4] *Department of Physics and Astronomy, Michigan State University, East Lansing, MI 48824, USA*

arXiv:1406.3634v1 [astro-ph.GA] 13 Jun 2014

17 June 2014

ABSTRACT
We study the effects of the external tidal field on the violent relaxation phase of star clusters dynamical evolution, with particular attention to the kinematical properties of the equilibrium configurations emerging at the end of this phase. We show that star clusters undergoing the process of violent relaxation in the tidal field of their host galaxy can acquire significant internal differential rotation and are characterized by a distinctive radial variation of the velocity anisotropy. These kinematical properties are the result of the symmetry breaking introduced by the external tidal field in the collapse phase and of the action of the Coriolis force on the orbit of the stars. The resulting equilibrium configurations are characterized by differential rotation, with a peak located between one and two half-mass radii. As for the anisotropy, similar to clusters evolving in isolation, the systems explored in this Letter are characterized by an inner isotropic core, followed by a region of increasing radial anisotropy. However for systems evolving in an external tidal field the degree of radial anisotropy reaches a maximum in the cluster intermediate regions and then progressively decreases, with the cluster outermost regions being characterized by isotropy or a mild tangential anisotropy. Young or old but less-relaxed dynamically young star clusters may keep memory of these kinematical fingerprints of their early dynamical evolution.

Key words: globular clusters: general

1 INTRODUCTION

Following the pioneering work of Lynden-Bell (1967) on the fundamental aspects of the evolution of stellar systems toward a virial equilibrium state, this phase of early relaxation of stellar systems (often referred to as violent relaxation) has been intensively investigated for systems spanning a broad range of physical scales and environments. A large number of studies have explored this process in the context of galaxy formation and early evolution (see e.g. Bertin 2000, Binney & Tremaine 2008 and references therein for reviews of the vast literature devoted to this topic).

Other studies have focussed their attention on star clusters (see e.g. Aarseth et al. 1988, Boily et al. 1999) and addressed a number of additional questions relevant to these smaller stellar systems. Examples include the possible connection between this dynamical phase and early mass segregation (see e.g. McMillan et al. 2007, Moeckel & Bonnell, 2009, Allison et al. 2009), the evolution of the number and orbital properties of primordial binary stars (Vesperini & Chernoff 1996, Kroupa et al. 1999, Kroupa & Burkert 2001, Parker et al. 2011), the dependence of the depth and dynamics of the initial collapse on the number of particles (Aarseth et al. 1988), the frequency and implications of stellar collisions (Fujii & Portegies Zwart 2013).

In studies of star cluster violent relaxation, the effects of the star cluster's host galaxy tidal field are rarely considered (Theis 2002; see also Boily & Pichon 2001 for a study of the effect of the host galaxy's torque on a triaxial star cluster). The goal of this Letter is to show how the dynamics of a star cluster during the violent relaxation phase and the kinematical properties of the equilibrium system emerging at the end of this process are affected by the host galaxy tidal field.

We will show that a cluster can acquire a significant differential rotation during the violent relaxation phase. In addition we will show that the velocity distribution anisotropy in isolated clusters and in clusters affected by the host galaxy tidal field differ significantly. Isolated stellar systems emerge from the violent relaxation phase with a velocity distribution increasingly radially anisotropic at larger distances from

© 0000 RAS

the center (see e.g. van Albada 1982, Trenti et al. 2005); in clusters affected by an external tidal field, the velocity anisotropy at the end of the violent relaxation phase is qualitatively similar to that of isolated clusters in the innermost (isotropic) and intermediate (radially anisotropic) regions but, in contrast with isolated clusters, the outer regions are characterized by an isotropic or a slightly tangentially anisotropic velocity distribution.

The outline of this Letter is the following. In Section 2 we describe the method and the initial conditions adopted in our study. In Section 3 we present our results. Section 4 summarizes our conclusions.

2 METHOD AND INITIAL CONDITIONS

For our investigation we have carried out a number of N-body simulations using the `starlab` package (Portegies Zwart et al. 2001) accelerated by a GPU (Gaburov et al. 2009).

The systems considered in this study are assumed to move on circular orbits in an external tidal field equal to either that of an isothermal halo or that of the local Galactic potential including the potential of the Galactic disk (assuming, in the latter case, an orbit on the plane of the Galactic disk at a distance from the Galactic center equal to that of the Sun).

In a coordinate system centered on the center of mass of the cluster and rotating around the Galactic center with constant angular velocity ω, with the x and y axes pointing away from the Galactic center and in the direction of motion respectively, the equations of motion for a star in the cluster, can be written in the tidal approximation as (see e.g. Heggie & Hut 2003)

$$\ddot{x_i} = F_x - \alpha_1 x_i + 2\omega\dot{y_i} \quad (1)$$

$$\ddot{y_i} = F_y - 2\omega\dot{x_i} \quad (2)$$

$$\ddot{z_i} = F_z - \alpha_3 z_i \quad (3)$$

where $(F_x,\ F_y,\ F_z)$ denote the force due to the other cluster stars, $\alpha_1 = -2\omega^2$ for an isothermal halo and $\alpha_1 = -4A(A-B)$ for the local Galactic disk field (where A and B are the Oort constants; see e.g. Heggie & Hut 2003), and $\alpha_3 = -0.5\alpha_1$ for the isothermal halo and $\alpha_3 = 4\pi G\rho_D + 2(A^2 - B^2)$ for the local Galactic disk (where ρ_D is the local density). All kinematical properties discussed in this Letter for clusters evolving in a tidal field, including those of initial conditions, are calculated in the rotating coordinate system introduced above (unless otherwise specified) and Eqs. 1-3 will be used in discussing the results of our simulations. In describing the rotational properties of the clusters, we will refer to prograde (retrograde) rotation to indicate rotation in the same sense as (opposite sense to) that of the cluster around the Galactic center (the rotational velocities calculated in the adopted rotating coordinate system are relative to the cluster initial synchronous solid-body rotation with angular velocity ω).

In addition to the cluster density profile, we characterize the initial conditions explored by using the virial ratio, $Q = T/|V|$ (where T is the total kinetic energy and V is the cluster internal potential energy), and the ratio of the cluster initial limiting radius to the Jacobi radius, R_L/R_J.

We have carried out four simulations starting with an equal-mass, spherical, homogeneous system, with a total number of particles $N = 60,000$, $R_L/R_J = 0.5$ and the following combinations of $(Q, \text{Tidal-Field})$: $(0.01, \text{Disk})$, $(0.1, \text{Disk})$, $(0.01, \text{Halo})$, $(0.01, \text{Isolated})$. Hereafter, we will refer to these simulations as, respectively, *CD* (Cold-Disk), *WD* (Warm-Disk), *CH* (Cold-Halo), *CI* (Cold-Isolated). The *CI* simulation has been included as a reference case to better illustrate the differences between the results obtained with and without an external tidal field. An additional simulation with an initial clumpy density distribution, $R_L/R_J = 0.5$ and $(Q, \text{Tidal-Field}) = (0.01, \text{Halo})$, hereafter referred to as *CCH* (Cold-Clumpy-Halo) has been run. The clumpy density distribution has been produced simply by letting the initial Poisson density fluctuations in an isolated homogeneous sphere grow until a time approximately equal to $0.97t_{ff}$ (where $t_{ff} = \sqrt{3\pi/(32G\rho)}$ is the free-fall timescale) and then resetting the virial ratio to the desired value for the initial conditions used for the simulation.

The units adopted are such that the total mass of the system, M, the gravitational constant G are equal to 1 and the initial limiting radius R_L is equal to about 1.2 . In these units the initial free-fall timescale is equal to about 1.45.

Particles moving beyond a radius equal to twice the Jacobi radius are removed from the simulation.

We point out that this Letter is aimed at discussing only the fundamental aspects of a star cluster violent relaxation in an external tidal field. A complete survey of simulations fully exploring the parameter space of initial structural and kinematical properties is currently in progress and will be presented in a separate paper.

3 RESULTS

Inspection of the equations of motions (eqs.1-3) discussed in the previous section, shows that the presence of an external tidal field and of the associated initial synchronous rotation adopted alters the collapse of a cold system in two ways. First, the cluster collapse is not isotropic: the collapse is accelerated in the z direction and slowed down in the x direction. Second, the Coriolis force affects the motion in the x and y directions by deflecting the star radial motion in prograde rotation during the collapse and in the opposite direction when the systems re-expands.

The first effect is shown in Fig.1. This figure illustrates the difference between the collapse of an isolated system (*CI*; lower panels) and that of a system affected by an external tidal field (*CD*; upper panels) by showing two snapshots at times around the moment of maximum contraction. While the *CI* system maintains its initial spherical symmetry, the *CD* system flattens in the z direction first (top left panel); as the re-expansion phase in the z direction starts the *CD* system is still collapsing in the $x-y$ directions (top right panel) producing a significant elongation in the z direction. In each panel, the inset shows the system projection on the $x-y$ plane.

The effect of the Coriolis terms in the equation of motion is illustrated in Fig. 2. This figure shows the time evolution of the radial profile of the rotational velocity around the z axis for the *CD* simulation and illustrates how the system

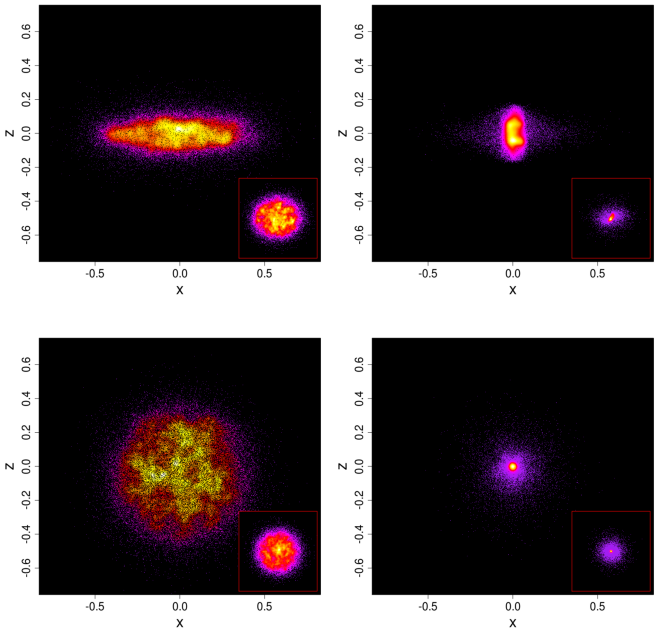

Figure 1. Snapshots of the simulations *CD* (top panels) and *CI* (bottom panels) at two times ($t \simeq 1.31$ left panels; $t \simeq 1.47$ right panels) close to the maximum contraction phase of the collapse. Particles are colored according to the local projected density (the density increases from purple to yellow) and in each panel the range of colors represents the range of densities at that time. Main figure in each panel shows the $x - z$ projection; each inset shows the $x - y$ projection.

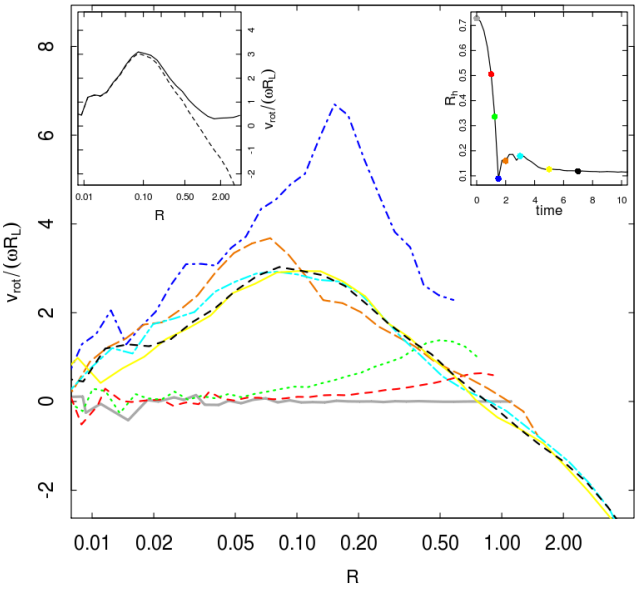

Figure 2. Radial profile of the rotational velocity, V_{rot} (normalized to the ωR_L where R_L is the cluster initial limiting radius and ω is the cluster angular velocity around the Galactic center), as a function of the cylindrical radius, R, for the *CD* simulation at $t = 0$ (grey solid line) $t = 1.0$ (red dashed line) $t = 1.25$ (green dotted line) $t = 1.5$ (blue dot-dashed line) $t = 2.0$ (orange long-dashed line) $t = 3.0$ (cyan long-short dashed line) $t = 5.0$ (yellow solid line) $t = 7.0$ (black dashed line). The radial profiles are calculated by dividing the system in cylindrical shells parallel to the z axis. The top left inset shows the rotation curve at $t = 7.0$, as measured in the non-rotating (solid line) and rotating (dashed line) coordinate systems. The top right inset shows the time evolution of the 2D half-mass radius with dots showing the times at which the radial profiles of V_{rot} in the main panel are calculated (the color scheme is the same as in the main panel). All the quantities presented in the panels are in N-body units.

acquires an internal differential rotational motion during the violent relaxation phase.

During the initial collapse, the whole system acquires a prograde differential rotation. After the maximum collapse phase, part of the system rapidly settles to form an inner high-density core in prograde rotation.

For shells of stars re-expanding and moving outward the Coriolis force acts in the direction opposite to that in which it acted during the collapse phase; this leads to a decrease in the rotational velocity of stars in the outer regions, with the outermost shells acquiring a significant retrograde rotation. The final rotational velocity profile is characterized by an inner rising portion, a peak in the cluster intermediate regions followed by a declining portion in the cluster outermost regions. We point out that, as already stated in §2, the rotational velocity profiles shown in Fig. 2 are calculated in the coordinate system synchronously rotating with the cluster orbital motion around the host galaxy. These profiles therefore show the development of the cluster differential rotation relative to the synchronous (angular velocity equal to the orbital ω) solid-body rotation. In the top left inset in Fig. 2 we also show one of the rotational velocity profiles calculated in the non-rotating coordinate system centered on the cluster center. Since the angular velocity of the cluster central regions is much higher than the angular velocity of the synchronous rotation ω, the inner rotational velocity profile is barely affected by this change of coordinates. In the outer regions the magnitude of the retrograde rotation in the rotating coordinate system is comparable to that of the synchronous solid-body rotation and, in the non-rotating system, the rotational velocity tends to small positive values (smaller than the synchronous rotational velocity). The rotational velocity profiles in the two coordinate systems both illustrate how, as a result of the collapse and the subsequent re-expansion during the violent relaxation phase the cluster acquires a differential rotational velocity significantly more (less) rapid than the initial synchronous rotation in its inner (outer) regions.

In Fig.3 we plot the radial profile of the ratio of the rotational velocity to the 1-D velocity dispersion, V_{rot}/σ, for all the simulations (the 1-D velocity dispersion is defined here as $\sigma = \sqrt{(\sigma_r^2 + \sigma_\theta^2 + \sigma_\phi^2)/3}$ as a function of the cylindrical radius R). All the systems discussed here are characterized by a similar shape of the radial V_{rot}/σ profile. As was to be expected, the less deep collapse of the cluster starting with a larger initial virial ratio (the *WD* simulation) leads to a final system characterized by smaller values of V_{rot}/σ. For all the systems the peak of V_{rot}/σ is located at a distance from the cluster center between R_h and $2R_h$ (where R_h is

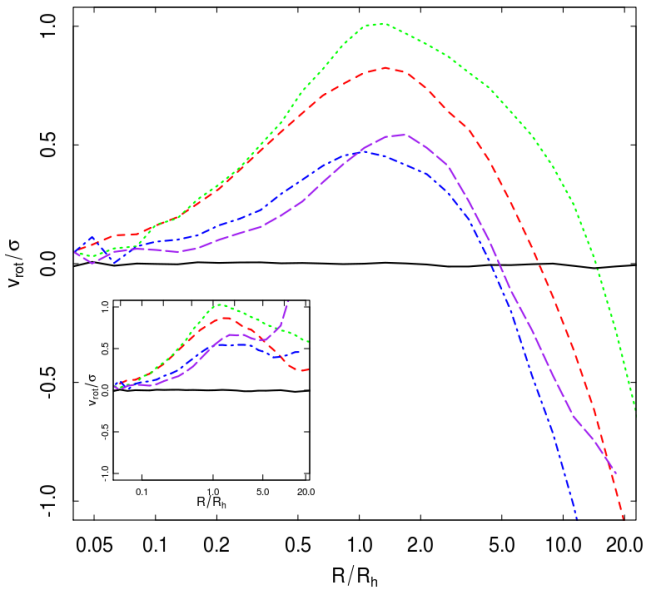

Figure 3. Radial profiles of the ratio of the rotational velocity around the z axis to the 1-D velocity dispersion, V_{rot}/σ, as a function of the ratio of the cylindrical radius to the projected half-mass radius, R/R_h, for the *CD* (red dashed line), *CH* (green dotted line), *WD* (blue dot-dashed line), *CCH* (purple long-dashed line), and *CI* (black solid line) simulations. The radial profiles shown are calculated by averaging the profiles at $5 \lesssim t/t_{ff} \lesssim 6.5$ (for the *CCH* system the profile was calculated by averaging profiles at $12 \lesssim t/t_{ff} \lesssim 13.5$ when there was no residual clumpiness in the cluster structure). The inset shows the profiles calculated in the non-rotating coordinate system.

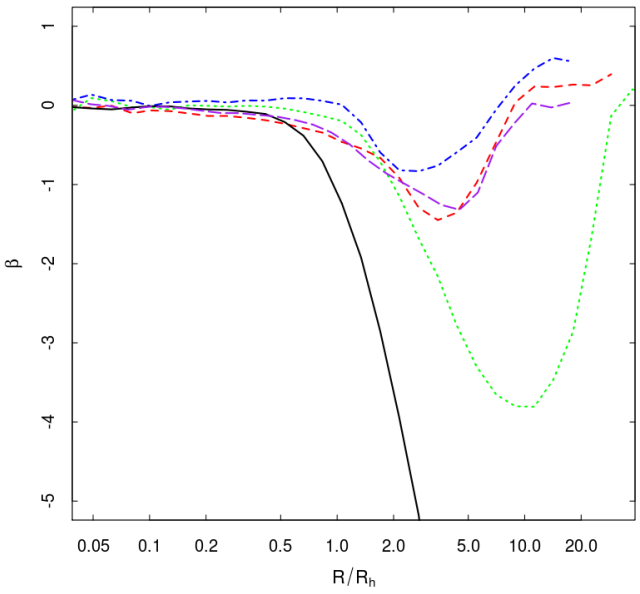

Figure 4. Radial profile of the anisotropy parameter β as a function of the ratio of the cyclindrical radius to the projected half-mass radius, R/R_h, for the *CD* (red dashed line), *CH* (green dotted line), *WD* (blue dot-dashed line), *CCH* (purple long-dashed line), and *CI* (black solid line) simulations. The radial profiles shown are calculated by averaging the profiles at $5 \lesssim t/t_{ff} \lesssim 6.5$ (for the *CCH* system the profile was calculated by averaging profiles at $12 \lesssim t/t_{ff} \lesssim 13.5$ when there was no residual clumpiness in the cluster structure).

the cluster projected half-mass radius). The radial profile of V_{rot}/σ for the isolated system (*CI*) is also shown in this figure and does not show any rotation. For completeness, as done in Fig. 2, we show in the inset the radial profiles of V_{rot}/σ calculated in the non-rotating coordinate system.

Finally in Fig.4 we plot for all the simulations the radial profiles of the anisotropy parameter $\beta = 1 - 2\sigma_r^2/(\sigma_\theta^2 + \sigma_\phi^2)$. For our *CI* simulation we recover the typical radial profile found at the end of violent relaxation of isolated systems; the system is characterized by an inner isotropic core and an increasingly radially anisotropic outer halo.

The systems evolving in an external tidal field are characterized by a qualitatively similar radial variation of β in the inner regions but the radial profiles of β for these systems deviate from that of an isolated system in the cluster outer regions. Specifically, for systems evolving in an external tidal field, β reaches a minimum and then rises again until the outermost shells where the system becomes isotropic or tangentially anisotropic. For the systems we have explored the position of the minimum in β is at a radius larger than $3R_h$; in units of the Jacobi radius the minimum of β is in all cases between $0.2R_J$ and $0.4R_J$.

It is interesting to notice that the behavior of the anisotropy parameter emerging from our simulations is qualitatively similar to the one observed in ω Cen (see van der Marel & Anderson 2010, van de Ven et al. 2006, and van Leeuwen et al. 2000). This observed kinematical property is particularly relevant to our study since ω Cen is characterized by a very long half-mass relaxation time and it therefore might be difficult to ascribe such a feature to the effects of long-term dynamical evolution (see e.g. Takahashi & Lee 2000, Baumgardt & Makino 2003, Hurley & Shara 2012 for some studies showing that tangential anisotropy in the outermost regions of star clusters can arise during their long-term evolution driven by two-body relaxation; in those cases the tangential anisotropy has been ascribed to the preferential loss of stars on radial orbits).

On the theoretical side, such a behaviour of the anisotropy parameter is also consistent with the kinematical properties of a family of self-consistent models with differential rotation presented by Varri & Bertin (2012) and recently applied to the dynamical interpretation of selected rotating Galactic globular clusters (Bianchini et al. 2013).

Finally we wish to emphasize that while the early collapse associated with the violent relaxation phase is necessary to produce the rapid inner rotation, the slow outer differential rotation found in our simulations could also arise during other dynamical phases driven by processes that cause the clusters to expand radially (for example, the radial expansion induced by mass loss due to stellar evolution).

4 CONCLUSIONS

We have studied the effects of the host galaxy tidal field on the dynamics of a star cluster violent relaxation. We have carried out a number of N-body simulations starting from initial conditions characterized by different density profiles, tidal fields, and different initial virial ratios.

We focused our attention on the kinematical properties of the equilibrium systems emerging at the end of the violent relaxation phase and we have shown that they differ significantly from those of systems undergoing this evolutionary phase in isolation. Specifically: 1) All the systems we have investigated acquire a significant differential rotation around the z axis during the violent relaxation phase and are characterized by final peak values of V_{rot}/σ between 0.5 and 1. Relatively to a reference coordinate system characterized by synchronous solid-body rotation (i.e. solid-body rotation with angular velocity equal to that of the cluster orbital motion around the host galaxy), the inner regions of the final equilibrium system rotate in the prograde direction (i.e. their rotational velocity is faster than the synchronous solid-body rotation) while stars in the outermost regions stars rotate in the opposite direction (i.e. their rotational velocity is slower than the synchronous solid-body rotation). The typical rotation velocity profile at the end of our simulations rises from the cluster center and reaches a maximum at a radius $R_{peak} \sim (1-2)R_h$. 2) The rapid inner rotation is acquired by the system during the collapse, while the subsequent re-expansion of the outer cluster shells is responsible for the outer slow rotation. While the initial collapse, typical of the first stages of evolution of a subvirial stellar system, is necessary to produce the inner rapid rotation, the outer slow differential rotation (slower than the synchronous solid-body rotation and, therefore, retrograde if measured relatively to the synchronously rotating coordinate system) can arise during other evolutionary phases driven by processes causing a radial expansion of the cluster (for example during the cluster expansion triggered by mass loss due to massive star evolution). 3) The presence of an external tidal field affects the radial profile of the velocity anisotropy. Similarly to clusters evolving in isolation, the systems explored in this Letter are characterized by an inner isotropic core, followed by a region of increasing radial anisotropy. However, for systems evolving in an external tidal field, the anisotropy parameter $\beta = 1 - 2\sigma_r^2/(\sigma_\theta^2 + \sigma_\phi^2)$ reaches a minimum (corresponding to a maximum in the radial anisotropy) and rises again in the outer regions with the outermost regions of the clusters characterized by isotropy or mild tangential anisotropy.

In this Letter, we have shown that significant differential rotation and a distinct radial variation of the anisotropy can emerge during a cluster early evolution. An extensive study of the dependence of the final equilibrium properties on the cluster initial density and rotational velocity profiles, virial ratio, concentration, and stellar mass spectrum is currently in progress and will be presented in a separate paper. To establish a connection between the kinematical properties identified in this study and those of dynamically old clusters, we are also currently exploring how these kinematical properties change during the cluster long-term evolution driven by two-body relaxation. Young or old but dynamically young clusters, on the other hand, might still keep memory of the kinematical fingerprints of this early evolution. High-precision proper motion studies of star clusters by means of HST and GAIA (see e.g. Bellini et al. 2013, Pancino et al. 2013) and ESO/VLT radial velocity studies (see e.g. Lanzoni et al. 2013) will help to shed light on the connection between their kinematical properties and their early and long-term dynamical history.

REFERENCES

Aarseth, S.J., Lin, D.N.C., Papaloizou, J.C.B., 1988, ApJ, 324, 288

Allison, R. J., Goodwin, S. P., Parker, R. J., de Grijs, R., Portegies Zwart, S. F., Kouwenhoven, M. B. N., 2009, ApJ, 700, L99

Baumgardt H., Makino J., 2003, MNRAS, 340, 227

Bellini, A., van der Marel, R. P., Anderson, J., 2013 *MmSAI*, 84, 140

Bertin, G., 2000, *Dynamics of Galaxies*, Cambridge University Press

Bianchini, P., Varri, A.L., Bertin, G., Zocchi, A., 2013, ApJ, 772, 67

Binney, J., Tremaine, S., 2008, *Galactic Dynamics*, Princeton University Press

Boily, C. Clarke, C.J., Murray, S.D., 1999, MNRAS, 302, 399

Boily, C. & Pichon, C., 2001, in *Dynamics of Star Clusters and the Milky Way*, ASPC, 228, p.392

Fujii, M.S., Portegies Zwart, S., 2013, MNRAS, 430, 1018

Gaburov, E., Harfst, S., Portegies Zwart, S., 2009, *New Astron.*, 14, 630

Heggie, D., Hut, P. 2003, *The Gravitational Million-Body Problem*, Cambridge University Press

Hurley, J., Shara, M., 2012, MNRAS, 425, 2872

Kroupa, P., Petr, M.G., McCaughrean, M.J., 1999, *New Astron.*, 4, 495

Kroupa, P. & Burkert, A., 2001, ApJ, 555, 945

Lanzoni, B. et al., 2013, ApJ, 769, 107

Lynden-Bell, D., 1967, MNRAS, 136, 101

McMillan, S.L.W, Vesperini, E., Portegies Zwart, S., 2007, ApJ, 665, L45

Moeckel, N., Bonnell, I.A., 2009, MNRAS, 400, 657

Pancino, E., Bellazzini, M., Marinoni, S, 2013, *MmSAI* 84, 83

Parker R. J., Goodwin, S. P., Allison, R. J., 2011, MNRAS, 418, 2565

Portegies Zwart, S., McMillan, S. L. W., Hut, P., Makino, J., 2001, MNRAS, 321, 199

Takahashi, K., Lee, H. M., 2000, MNRAS, 316, 671

Theis, C., 2002, *Ap&SS*, 281, 97

Trenti, M., Bertin, G., van Albada, T.S., 2005, A&A, 433, 57

van Albada, T.S., 1982, MNRAS, 201, 939

van de Ven, G., van den Bosch, R. C. E., Verolme, E. K., de Zeeuw, P. T., 2006, A&A, 445, 513

van der Marel, R. P., Anderson, J., 2010, ApJ, 710, 1063

Varri, A.L., Bertin, G., 2012, A&A, 540, A94

Vesperini, E., Chernoff D.F., 1996, ApJ, 458, 178